



Older than you think: using U–Pb calcite geochronology to better constrain basin-bounding fault reactivation, Inner Moray Firth Basin, western North Sea

A. Tamas^{1,2*}, R. E. Holdsworth^{2,3}, D. M. Tamas¹, E. D. Dempsey⁴, K. Hardman⁴, A. Bird⁴, N. M. W. Roberts⁵, J. Lee², J. R. Underhill⁶, D. McCarthy⁷, K. J. W. McCaffrey^{2,3} and D. Selby²

¹ Centre for Integrated Geological Studies, Babes-Bolyai University, Cluj-Napoca, Romania

² Department of Earth Sciences, Durham University, Durham, UK


³ Geospatial Research Ltd, Durham, UK

⁴ Department of Geology, Hull University, Hull, UK

⁵ Geochronology and Tracers Facility, British Geological Survey, Nottingham, UK

⁶ School of Geosciences, University of Aberdeen, Aberdeen, UK

⁷ British Geological Survey, Edinburgh, UK

 AT, 0000-0001-8010-1853; REH, 0000-0002-3467-835X; DMT, 0000-0002-6640-8928; EDD, 0000-0002-8425-2226; AB, 0000-0002-2496-4344; NMWR, 0000-0001-8272-5432; JL, 0000-0001-8435-3484; DM, 0000-0002-0677-773X; KJWM, 0000-0002-9882-1709

*Correspondence: alexandra.tamas1@ubbcluj.ro

Abstract: Like many rift basins worldwide, the Inner Moray Firth Basin (IMFB) is bounded by major reactivated fault zones, including the Helmsdale Fault and the Great Glen Fault (GGF). The Jurassic successions exposed onshore close to these faults at Helmsdale and Shandwick preserve folding, calcite veining and minor faulting consistent with sinistral (Helmsdale Fault) and dextral (GGF) transtensional movements. This deformation has been widely attributed to Cenozoic post-rift fault reactivation. Onshore fieldwork and U–Pb calcite geochronology of five vein samples associated with transtensional movements along the Helmsdale Fault and a splay of the GGF show that faulting occurred during the Early Cretaceous (*c.* 128–115 Ma, Barremian–Aptian), while the Helmsdale Fault preserves evidence for earlier Late Jurassic sinistral movements (*c.* 159 Ma, Oxfordian). This demonstrates that both basin-bounding faults were substantially reactivated during the episodic NW–SE-directed Mesozoic rifting that formed the IMFB. Although there is good evidence for Cenozoic reactivation of the GGF offshore, the extent of such deformation along the north coast of the IMFB remains uncertain. Our findings illustrate the importance of oblique-slip reactivation processes in shaping the evolution of continental rift basins given that this deformation style may not be immediately obvious in interpretations of offshore seismic reflection data.

Supplementary Material: Appendix A – orthomosaic model obtained from unmanned aerial vehicle (UAV) photography of the Helmsdale locality (GeoTiff format); Appendix B – orthomosaic model obtained from UAV photography of the Shandwick locality (GeoTiff format); Appendix C – geochronology data; and Appendix D – additional thin section microphotographs of sample HD1 showing repeated cycles of syntaxial grain growth are available at <https://doi.org/10.6084/m9.figshare.c.6708518>

Received 21 November 2022; revised 13 June 2023; accepted 19 June 2023

Basin-bounding faults have key roles in controlling basin development and geometry, accommodation space, sediment pathways and fluid flow (Salomon *et al.* 2020). These faults are commonly reactivated during later episodes of rifting or inversion, leading to complex localized deformation zones (e.g. Worthington and Walsh 2016; Dichiarante *et al.* 2020) that can affect the development of subsurface resources and applications (e.g. minerals, hydrocarbons, geothermal energy and CO₂ storage). In many cases, the timing of basin-bounding fault movements may be difficult to constrain due to the limited resolution of seismic data in offshore regions, while onshore areas may have restricted surface exposures and a lack of stratigraphic constraints.

The Inner Moray Firth Basin (IMFB) is widely regarded as a classic example of an intracontinental rift zone (e.g. Underhill 1991). Existing models suggest that the reactivation of two older basement structures, the Helmsdale Fault and the Great Glen Fault (GGF) had a key role in the Mesozoic–Cenozoic development of the IMFB, both during rifting and subsequent regional inversion. We use new field observations and microstructural observations to constrain U–Pb dating of the calcite mineralization associated with

deformation along the onshore parts of the Helmsdale Fault and a splay of the GGF. These results demonstrate that the main phases of reactivation of these onshore faults were mainly pre-Cenozoic and related to rifting. These movement ages are older than has been proposed previously (e.g. Thomson and Underhill 1993; Le Breton *et al.* 2013) and significantly change our understanding of the evolution of the IMFB. This work also illustrates the value of U–Pb calcite dating to better constrain the timing of regional fault displacements (e.g. Roberts and Holdsworth 2022).

Geological setting

The GGF and Helmsdale Fault are major fault zones that, together with the Banff and Wick faults, bound the IMFB in NE Scotland (Fig. 1a, b). The basin rests on Precambrian–Caledonian metamorphic basement and Devonian–Carboniferous sedimentary rocks related to the older and much larger Orcadian Basin (Fig. 1a, c). From the Permian to Cretaceous, the basin formed the western arm of the intracontinental North Sea trilete rift system (McQuillin *et al.* 1982; Andrews *et al.* 1990; Underhill 1991). Subsequently, the

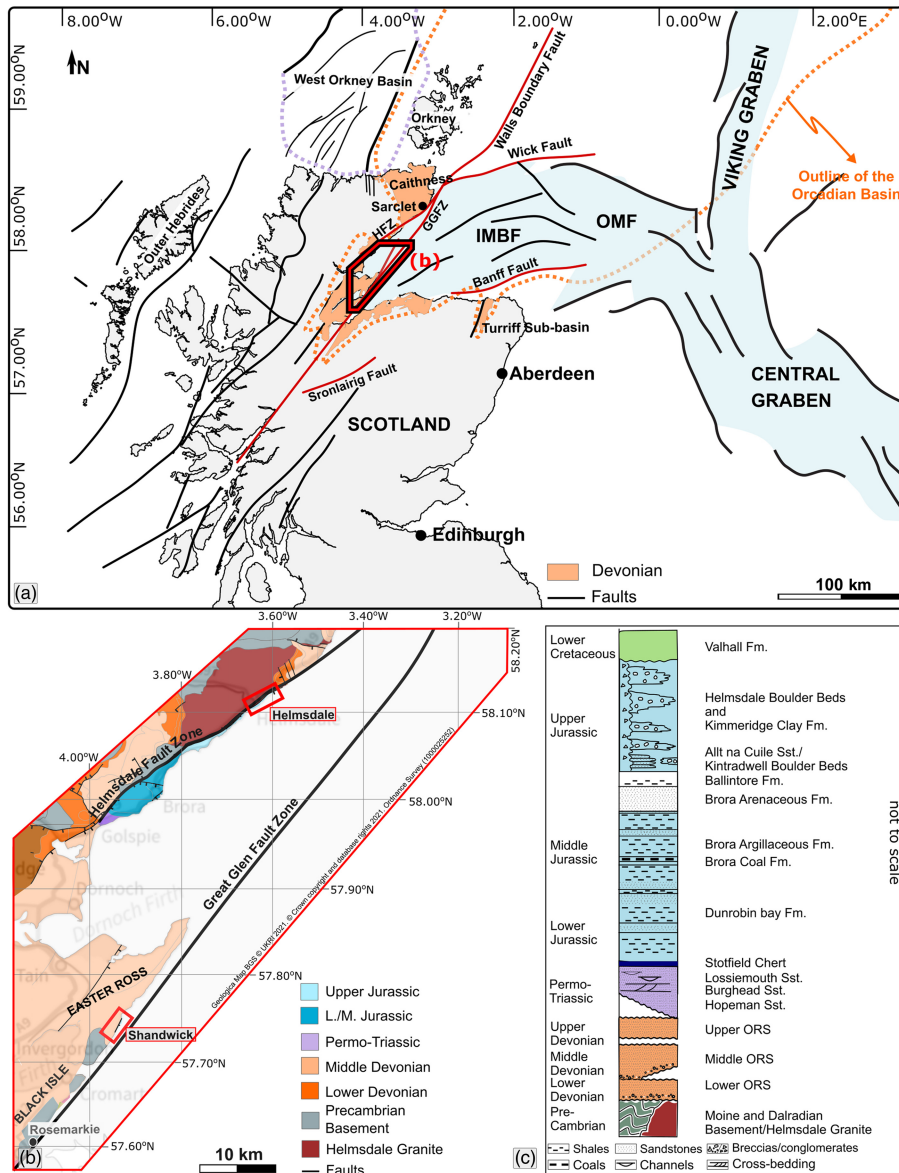


Fig. 1. (a) Tectonic map of Scotland and the Northern North Sea region showing the main fault systems. The faults mentioned in the text are shown in red. The outline of the Orcadian Basin is marked by the dotted orange line and the outline of the West Orkney Basin is marked by the dotted purple line; the red box shows the location of part (b). (b) Simplified regional geological map of the northwestern coast of the Inner Moray Firth Basin showing onshore study areas (red boxes). (c) Summary of onshore stratigraphy (modified after [Trewin and Hurst 2009](#)). Not to scale, with notional relative thicknesses shown. GGFZ, Great Glen Fault Zone; HZF, Helmsdale Fault Zone; IMBF, Inner Moray Firth Basin; OMF, Outer Moray Firth; ORS, Old Red Sandstone. Source: part (a) from [Tamas *et al.* \(2022a\)](#).

IMFB is widely considered to record important episodes of Late Cretaceous–Cenozoic regional uplift and faulting, including dextral reactivation of the GGF and sinistral reactivation of the Helmsdale Fault (e.g. [Underhill 1991](#); [Thomson and Underhill 1993](#); [Le Breton *et al.* 2013](#)).

Helmsdale Fault

The Helmsdale Fault is a c. 100 km long NE–SW-striking, steeply SE-dipping fault ([Figs 1b, 2a](#)) that runs onshore for about half of its length. An almost continuous succession of Triassic–Upper Jurassic basin-fill rocks is exposed onshore in its hanging wall ([Fig. 1b, c](#)), downfaulted to the SE against basement rocks of the Moine Supergroup, Helmsdale Granite and Devonian successions to the NW ([Fig. 1b](#); [BGS 1998](#); [Trewin 2009](#)). The Helmsdale Fault acted as a normal fault during Late Jurassic–Early Cretaceous basin opening (e.g. [Underhill 1991](#); [Thomson and Underhill 1993](#)). The Upper Jurassic synrift succession is well exposed on the coast at Helmsdale ([Figs 1b, c](#) and [2](#)), where deep marine fault scarp deposits known as the ‘Boulder Beds’ were deposited (e.g. [Bailey and Weir 1932](#); [Pickering 1984](#); [McArthur *et al.* 2013](#)). This sequence is folded by 500 m wavelength, NW–SE-trending open folds ([Fig. 2b, c](#)), consistent with sinistral shear along the Helmsdale Fault ([MacDonald 1985](#); [Thomson and Underhill 1993](#); [Thomson and](#)

[Hillis 1995](#)). Because the synrift faults were considered to be dip-slip (e.g. [Underhill 1991](#)), this strike-slip/oblique movement along the Helmsdale Fault has been related to a later episode of reactivation during the Cenozoic, coeval with the dextral displacement of the GGF and regional uplift and tilting of the IMFB to the ESE ([Thomson and Underhill 1993](#); [Hillis *et al.* 1994](#); [Le Breton *et al.* 2013](#)). Regionally, the post-Devonian faulting histories on either side of the Helmsdale Fault appear to differ significantly, suggesting that the fault acted as a regional boundary that restricted the effects of Mesozoic faulting to the interior parts of the IMFB ([Dichiarante *et al.* 2016](#)).

Great Glen Fault

The NE–SW-trending GGF ([Fig. 1a](#)) initiated as a subvertical, crustal-scale sinistral fault in the mid-Silurian (c. 425 Ma; e.g. [Stewart *et al.* 2001](#)). During the opening of the Orcadian Basin, the fault had an initial left-lateral movement (e.g. [Dewey and Strachan 2003](#); [Mendum and Noble 2010](#)), whereas it is thought to have been reactivated dextrally in the Late Carboniferous–Early Permian (e.g. [Holgate 1969](#); [Coward *et al.* 1989](#)). It forms the NW margin of the IMFB on the Black Isle and in Easter Ross ([Fig. 1b](#)) running northeastwards into the basin, intersecting the Helmsdale Fault and ultimately linking to the Walls Boundary Fault in Shetland ([Fig. 1a](#); [Watts *et al.* 2007](#)).

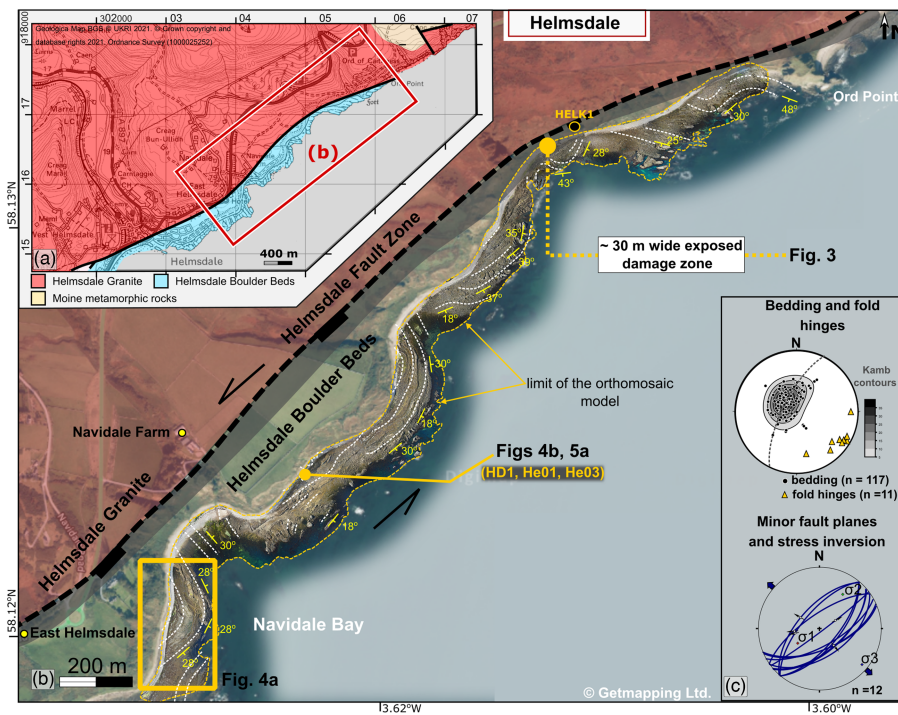


Fig. 2. (a) Geological map of the Helmsdale area (using EdinaDigimap service and BGS 1998) showing the location of part (b). Orthomosaic model obtained from unmanned aerial vehicle photography overlapped on an aerial map (using EdinaDigimap service © Getmapping plc) of the studied exposures. Locations of samples and of Figures 4, 5a, b and 6a are indicated. (c) Stereonets and rose plots of structural data collected in the field. Lower hemisphere, equal-area projections.

The GGF was initially considered to have been reactivated as a dextral transtensional basin-controlling structure during Mesozoic rifting (e.g. McQuillan *et al.* 1982; Roberts *et al.* 1990). However, later interpretations of seismic reflection data suggested that the GGF was inactive during the Late Jurassic–Early Cretaceous. Underhill (1991) proposed that the IMFB opened mainly during the Late Jurassic under an orthogonal extensional regime. The main displacements were interpreted to lie along the Helmsdale Fault because the synkinematic sequence thickens without change across the GGF and towards the Helmsdale Fault.

Subsequent studies (e.g. Thomson and Underhill 1993; Underhill and Brodie 1993; Davies *et al.* 2001) demonstrated that the GGF and associated faults show evidence for younger strike-slip-related deformation patterns (e.g. the development of flower structures and folds) that clearly offset post-rift reflectors on the offshore seismic reflection profiles. Hence the later dextral reactivation of the GGF is now widely regarded as occurring in the Cenozoic (e.g. Underhill and Brodie 1993; Le Breton *et al.* 2013).

A splay of the GGF is exposed onshore along the Easter Ross and Black Isle coast (Fig. 1b), juxtaposing Jurassic strata to the east against Devonian and Precambrian metamorphic basement rocks to the west. Minor folds and faults in the Jurassic strata here are considered to be Cenozoic and related to right-lateral slip along the GGF (e.g. Underhill and Brodie 1993). It is generally believed by these researchers that the GGF reactivated right-laterally in a time interval from the Late Eocene to Late Oligocene at *c.* 37–26 Ma (Le Breton *et al.* 2013).

Calcite veins

Calcite veins have been described from the Jurassic rocks associated with the onshore exposures close to both the Helmsdale Fault and the GGF (e.g. MacDonald 1985; MacDonald and Trewin 2009). These veins are generally considered to have formed after the host sedimentary rocks were fully lithified and also to be later, and unrelated to, the folds seen in the hanging wall of the Helmsdale Fault (MacDonald 1985). Le Breton *et al.* (2013) view their formation as being related to Cenozoic deformation and fluid flow. The present study re-examines the structural relationships of the veins in the field and thin section to better ascertain the age of calcite precipitation relative to deformation in the host country rocks. We

then use the U–Pb geochronology of selected samples to date the absolute ages of the basin-controlling fault movements along the Helmsdale Fault and GGF splay.

Methodology

Structural fieldwork and sampling were carried out along the coastal sections at Helmsdale (the Helmsdale Fault) and at Shandwick (the GGF splay; Fig. 1b). The grid references used refer to the British National Grid. Detailed observations and structural measurements were recorded during fieldwork. Structural data processing and visualization were carried out using Stereonet 10 (lower hemisphere, equal-area projections; Cardozo and Allmendinger 2013). Where appropriate, fault-slip slickenline data were collected to perform palaeostress inversions using the direct inversion method of Angelier (1990) implemented in SG2PS software (Sasvári and Bahrev 2014). Unmanned aerial vehicle photographs were collected using a DJI Mavic Air drone. We used Agisoft Metashape Professional (v.1.6.2) to create digital outcrop models and orthorectified models; the workflow is detailed in Tamas *et al.* (2021). The high resolution orthorectified models are available as GeoTiff files in the Supplementary Material, Appendices A and B. The orthorectified models were overlapped onto the aerial maps. These maps were obtained using the EDINA Digimap service, which provides access to high-quality 25 cm vertical orthophotography available for Great Britain, created and licensed by Getmapping plc.

For the geochronology, calcite-filled fracture samples were collected for microstructural and geochronological studies. Polished chips or thick sections were analysed using laser ablation inductively coupled plasma mass spectrometry at the Geochronology and Tracers Facility, British Geological Survey (Nottingham, UK) and the University of Hull (Hull, UK) using the methods for calcite U–Pb geochronology outlined in Roberts *et al.* (2017) for the British Geological Survey samples and Holdsworth *et al.* (2020) for the University of Hull samples. The analytical conditions and data are provided in the Supplementary Material, Appendix C.

The calcite samples are characterized by low U and Pb concentrations (average 1.09 and 2.62 ppm, respectively). As a result, some laser spot analysis resulted in poor data acquisition and significant uncertainties on the low-sensitivity quadrupole

instrumentation at the University of Hull. As well as removing data below the reliable detection limits, data with uncertainties $>20\%$ 2s on the $^{238}\text{U}/^{206}\text{Pb}$ ratios and 10% 2s on the $^{207}\text{Pb}/^{206}\text{Pb}$ ratios were not utilized in the final date calculation. This did not have a significant effect on the final ages. The ages were calculated as lower intercept $^{238}\text{U}/^{206}\text{Pb}$ ages with uncertainties quoted at 2s and include the propagation of systematic uncertainties; these include the 2.5% uncertainty of the WC1 reference material and a conservative estimate of the long-term reproducibility of 2%. Initial Pb compositions (upper intercepts) are provided in the summary table in the [Supplementary Material, Appendix C](#). All data plotting and age calculations used IsoplotR (Vermeesch 2018) and the ellipses represent 2σ uncertainties.

Field and microstructural observations

Helmsdale

The Helmsdale coastal outcrops follow the trace of the Helmsdale Fault, exposing Upper Jurassic Boulder Beds downfaulted to the SE

against the late Silurian Helmsdale Granite (Fig. 2a, b; Pickering 1984; Thomson and Underhill 1993; Macdonald and Trewin 2009). The section studied here extends c. 2.5 km from East Helmsdale [ND 04068 15596] to Ord Point [ND 05864 17209]. The Boulder Beds here consist of decimetre to metre thick breccias formed by angular/subangular clasts of mostly locally derived Devonian sandstones. The breccias are interbedded with thin-bedded (millimetres to centimetres thick) light and dark grey sandstones and laminated dark shales. Slump folds, very large Devonian blocks (metres wide) and sandstone intrusions are also present within the Boulder Beds. These deposits are widely interpreted to be debris flow breccias triggered by the syn-sedimentary movements along the Helmsdale Fault and to the development of an associated surface fault scarp (e.g. Pickering 1984; McArthur *et al.* 2013).

The main slip plane of the Helmsdale Fault is not exposed, but a c. 30 m wide deformation zone in the hanging wall of the fault is preserved cutting the Boulder Beds (Figs 2b, 3). Here, 50 cm to 1 m wide yellow–orange fault gouge/breccia (Fig. 3a), together with NE–SW-trending cataclasites (Fig. 3b) and minor SE- and NW-dipping minor faults (Fig. 3c–e) occur. Kinematic indicators on slip



Fig. 3. Field photographs of structures within the Helmsdale Fault damage zone [ND 05172 17046]. (a) Yellow/orange fault gouge. (b) NE–SW-trending strands of deformation bands shown in red (also without interpretation in the inset). (c) Minor antithetic fault plane (dipping to the NW). (d) Kinematic indicators on exposed minor faults showing dip-slip to slightly sinistral-normal oblique-slip movements. (e) Minor synthetic fault plane (dipping to the SE).

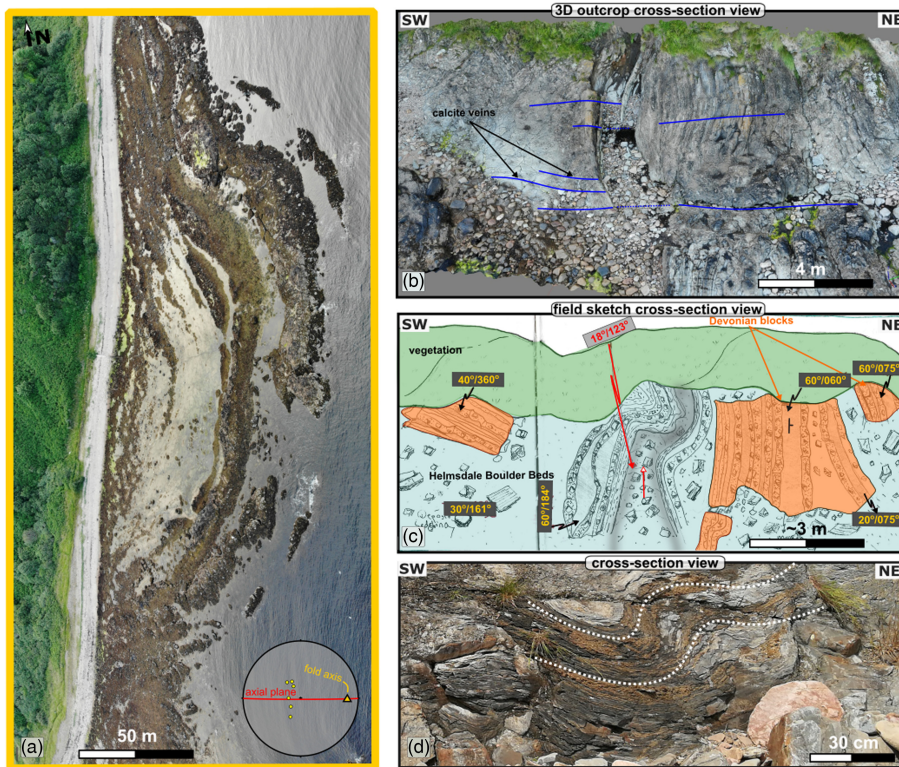


Fig. 4. (a) Drone image of the large-scale fold at Navidale Bay [ND 04190 15778] and inset stereonet of the folded bedding planes, hinges and fold axial plane (see Fig. 2b for location). (b) 3D model and (c) field sketch constructed in the same location as part (b) showing small-scale folding and cross-cutting calcite veins [ND 04494 16213]. The bedding measurements (in yellow) are provided as dip/dip directions. (d) Field photograph of small-scale fold within the Boulder Beds. These folds are shallowly plunging to the SE, similar to the large-scale folds. Also note the large Devonian clasts (orange overlay) with the bedding dipping at different angles within the Boulder Beds in part (c).

planes show dip-slip/sinistral-normal oblique-slip (e.g. Fig. 3d), which palaeostress inversion suggests are consistent with NW–SE transension (Fig. 2c).

Next to the fault zone, the Upper Jurassic strata are deformed by shallowly SE- to east-plunging ($6\text{--}18^\circ$) open folds on metre to decimetre scales (Figs 2c and 4a–d). The folds are cross-cut by 7–10 m wide clusters of calcite-mineralized tensile veins that extend laterally up to 100 m (Figs 4b and 5a–e). The veins are steeply NW-dipping ($>60^\circ$), sub-millimetre to 10 cm wide, NE–SW-trending features that run sub-parallel to the Helmsdale Fault (Fig. 5b). Some of the wider veins are incompletely sealed and have large (millimetre–centimetre) euhedral crystals lining open vugs (e.g. Fig. 5d). The widespread veins also cross-cut the Helmsdale Granite in the footwall of the Helmsdale Fault and, in the hanging wall, both the matrix of the Boulder Beds (Fig. 5a, d) and clasts of Devonian and Moine basement (Fig. 5a, e). Calcite fills were sampled both from close to the Helmsdale Granite (HELK01; Fig. 5c, f) and in the main outcrop of the folded Upper Jurassic Boulder Beds (HD1 and He03; Fig. 5a, d). One sample (He01) displays early pink calcite veins seen only in Devonian sandstone clasts that are cross-cut by the white calcite veins that also transect the surrounding matrix of the Boulder Beds.

The HELK01 sample is a carbonate-cemented proximal fault scarp sedimentary breccia containing large clasts of granite (Fig. 5f, g). It is cross-cut by calcite–siderite-filled tensile veins (Fig. 5h), one of which was dated in this work. Later clear calcite fills, which were not dated in this work, follow these pre-existing calcite–siderite veins.

The HD1 sample (Fig. 6a) comes from a NE–SW-trending 10 cm thick calcite vein (Fig. 5d) with composite syntaxial fills coarsening inwards to give ‘beef-like’ textures (Fig. 6a, b). The elongation of crystals is normal to the tensile fracture walls. Some fills show evidence of past vugs that are occluded, leading to repeated cycles of syntaxial grain growth, whereas others comprise simpler single growths (see images described in Supplementary Material, Appendix D).

The He01 sample (Fig. 6c) was collected from a Devonian sandstone boulder within the Boulder Beds (Fig. 5e). Early pink

calcite veins (only seen in Devonian clasts) are cut by pale white calcite veins (Fig. 6d), which also cut the Boulder Beds matrix. The pink veins are therefore demonstrably pre-Jurassic. The pink veins have notably irregular margins and are everywhere cut by pale white veins with calcite fills, the latter growing in optical continuity with crystals in older veins (Fig. 6d). The later set were dated in this work and locally host fresh hematite (Fig. 6d).

The He03 sample shows three sets of white calcite veins (Fig. 6e–i). Early thin (<1 mm) fine-grained fills with irregular margins (set i, Fig. 6f, g) are cut by a predominant set of feathered crack-seal veins (set ii, Fig. 6f, h; dated in this work) and later coarser sparry white calcite fills with central open fractures (set iii, Fig. 6f, i).

Shandwick

The studied coastal section lies *c.* 200 m south of Shandwick [NH 857 745] and extends *c.* 1 km northwards from Port an Righ (Fig. 7a, b). The Upper Jurassic rocks here form a narrow strip in the wave-cut platform, downfaulted to the SE against Middle Devonian strata (Fig. 7a). This NNE–SSW-striking fault is considered to be a splay of the GGF (e.g. Underhill and Brodie 1993; Le Breton *et al.* 2013). The Devonian rocks in the footwall of the GGF splay form extensive rock platforms and cliffs to the north and south of the study area. They consist of gently NE-dipping ($20\text{--}30^\circ$) thin-bedded (5–20 cm) dark red sandstones, which are fine grained and very well cemented.

The Upper Jurassic rocks exposed in the hanging wall of the GGF splay belong to stratigraphic members of the Brora Argillaceous (Shandwick Clay Member), Brora Arenaceous (Shandwick Siltstone Member) and Balintore formations (Port an Righ Ironstone and Siltstone members) (Fig. 1c; Riding 2005). The strata consist of centimetre to decimetre thick grey–green mudstones, sandstones, and limestones rich in marine fossils (such as ammonites and large bivalves). These are thought to have accumulated in a distal shelf environment (Stephen *et al.* 1993; Riding 2005). A very distinct layer *c.* 2–2.5 m thick of thin-bedded (10–20 cm) red-weathered fossiliferous limestones interbedded

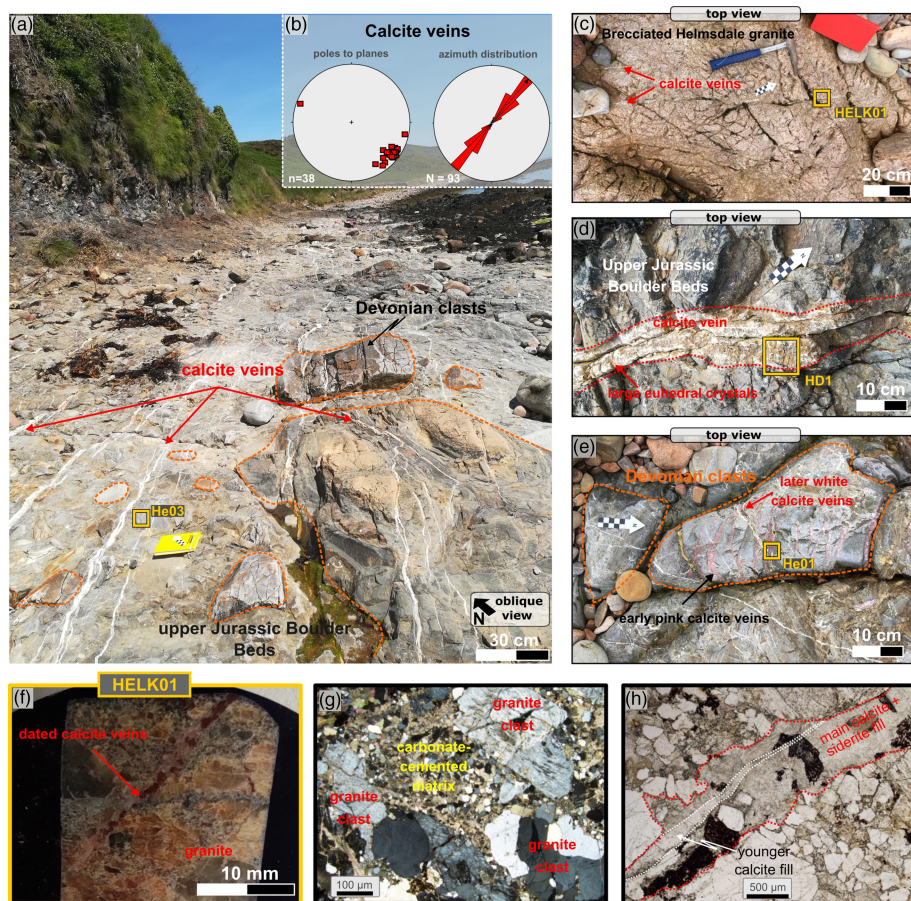


Fig. 5. (a) Field photograph showing calcite-mineralized tensile veins cross-cutting the Upper Jurassic Boulder Beds [ND 04491 16211]. Note that the Devonian boulders are also cross-cut by calcite veins. The location of sample He03 is also indicated. (b) Stereonet (lower hemisphere, equal-area projection) and rose plot of the calcite-mineralized veins. (c) Field photograph showing calcite-mineralized tensile veins cross-cutting a fault scarp breccia with abundant Helmsdale Granite clasts [ND 05188 17078]. The location of sample HELK01 is also indicated. (d) Close-up image of a wide (*c.* 10 cm) calcite vein with location of sample HD1 also shown. (e) Field photograph of a Devonian clast within the Upper Jurassic Boulder Beds cross-cut by early pink calcite veins and later white calcite veins. (f) Polished thick section of the HELK01 sample. (g) Representative thin section photomicrographs of HELK01 sample showing the granite clasts lying in a carbonate-cemented matrix (crossed polarized light). (h) Thin section photomicrographs of HELK01 sample showing a calcite and siderite vein similar to the one dated here. Note the younger cross-cutting calcite vein following the earlier mineral fill (plane polarized light).

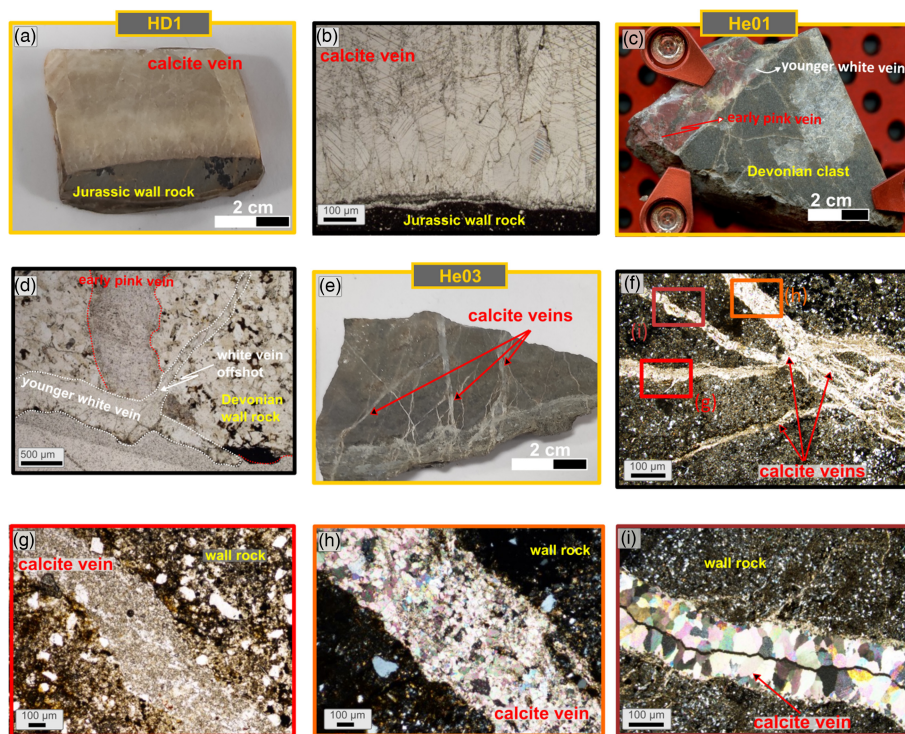


Fig. 6. (a) Polished thick section of the HD1 sample. (b) Representative thin section photomicrograph of HD1 sample in plane polarized light showing elongated calcite crystals with 'beef-like' textures. The elongation of the crystals is normal to the tensile fracture walls. (c) Polished thick section of the He01 sample showing the earlier pink calcite veins and later white calcite veins cross-cutting the Devonian clast. (d) Representative thin section photomicrographs of He01 sample showing the pink veins with irregular margins cut by pale white veins, with the later calcite fills growing in optical continuity with the crystals in older veins (plane polarized light). (e) Polished thick section of the He03 sample. (f–i) Representative thin section photomicrographs of the He03 sample (crossed polarized light) showing at least three sets of veins recognized by differences in texture and cross-cutting relationships. (g) Early set i veins, which are thin (<1 mm), yellowish and fine grained with irregular margins and lack internal structure. (h) Set ii veins, which are wispy, feathered veins with crack-seal textures and mostly white calcite fine sparry fills. (i) Set iii veins, which are coarser sparry white calcite with central open fractures that typically follow the earlier set ii veins.

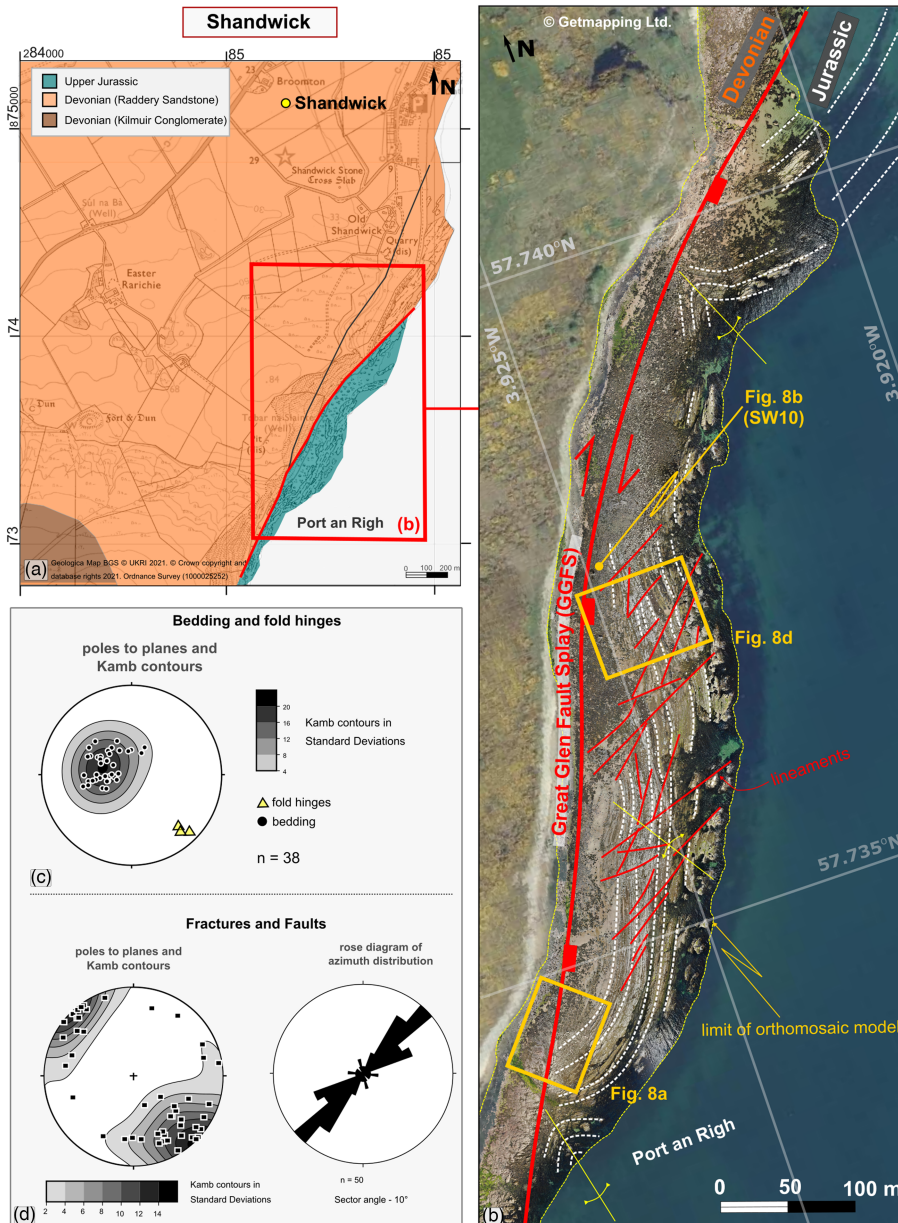


Fig. 7. (a) Geological map of the Shandwick area (using EdinaDigimap service) showing the location of part (b). (b) Orthomosaic model obtained from unmanned aerial vehicle photography overlapped on an aerial map (using EdinaDigimap service © Getmapping plc) of the studied exposure. Locations of Figure 8a, b and d are indicated. Stereonets and rose plots of structural data collected in the field: (c) bedding and (d) fractures and faults. Lower hemisphere, equal-area projections.

with grey mudstone and siltstones is known locally as the Port an Righ Ironstone (Stephen *et al.* 1993; Riding 2005; Duxbury and Vieira 2018). This forms a prominent stratigraphic marker that aids in identifying fault displacement senses where it is offset.

The Upper Jurassic beds in the hanging wall of the GGF splay fault dip shallowly to moderately SE (c. 12–47°, Fig. 7b, c) and are folded into large, gentle (interlimb angle c. 140°) upright folds plunging shallowly (10–23°) SE (Fig. 7c). The main NNE–SSW fault surface (Figs 7b, 8a) is unexposed, but a c. 2–5 m wide, sub-parallel calcite-mineralized fault zone (Fig. 8b) is preserved in the Jurassic rocks. The faults and fractures are NNE–SSW- to ENE–WSW-trending (Fig. 7d) and are generally steeply dipping (56–70°). A sample (SW10; Fig. 8b) was collected from a mineralized slip plane.

Throughout the Upper Jurassic strata, steeply dipping, millimetre to centimetre wide, ENE-trending tensile veins also occur, consistent with NNW–SSE extension (Fig. 8c and inset). Other, more NE–SW-trending, faults show centimetre- to metre-scale dextral offsets of bedding in the Upper Jurassic strata, including a 60 m offset of the Port an Righ Ironstone (Fig. 8d). These right-lateral faults are interpreted to be synthetic structures because they strike at c. 10–25° to the main fault. Striated minor faults trending ESE–WNW and dipping between 56° and 88° show oblique-

sinistral kinematics (lineation rakes of 28–50° W) and are interpreted as antithetic structures. A stress inversion analysis of slickenlines associated with these minor faults yields a NW–SE extension direction (Fig. 8e), consistent with an extension-dominated transtensional strain (De Paola *et al.* 2005). In summary, all the minor dextral and sinistral faults, tensile veins and folds in the Jurassic rocks at Shandwick seem to be genetically related to the GGF splay fault. They most likely represent a well-developed Riedel shear system associated with dextral-normal displacements along that structure (Fig. 8f).

The SW10 sample (Fig. 9a) comes from a NNE–SSW-trending minor fault within the main dextral-normal fault zone (Fig. 8b) that juxtaposes Devonian rocks in its western footwall with Upper Jurassic rocks in its eastern hanging wall (Fig. 7). The calcite fills in the SW10 sample both predate and post-date faulting and are kinematically consistent with dextral shear because they are associated with right-lateral dilational jogs (Fig. 9b). Clasts in high strain areas have developed obliquely oriented pressure shadows consistent with dextral shear (Fig. 9c), whereas earlier fills are cataclastically deformed and show stylolitic contacts consistent with shortening at high angles to the fault planes (Fig. 9c–e). The later cross-cutting sparry vein fills, which were

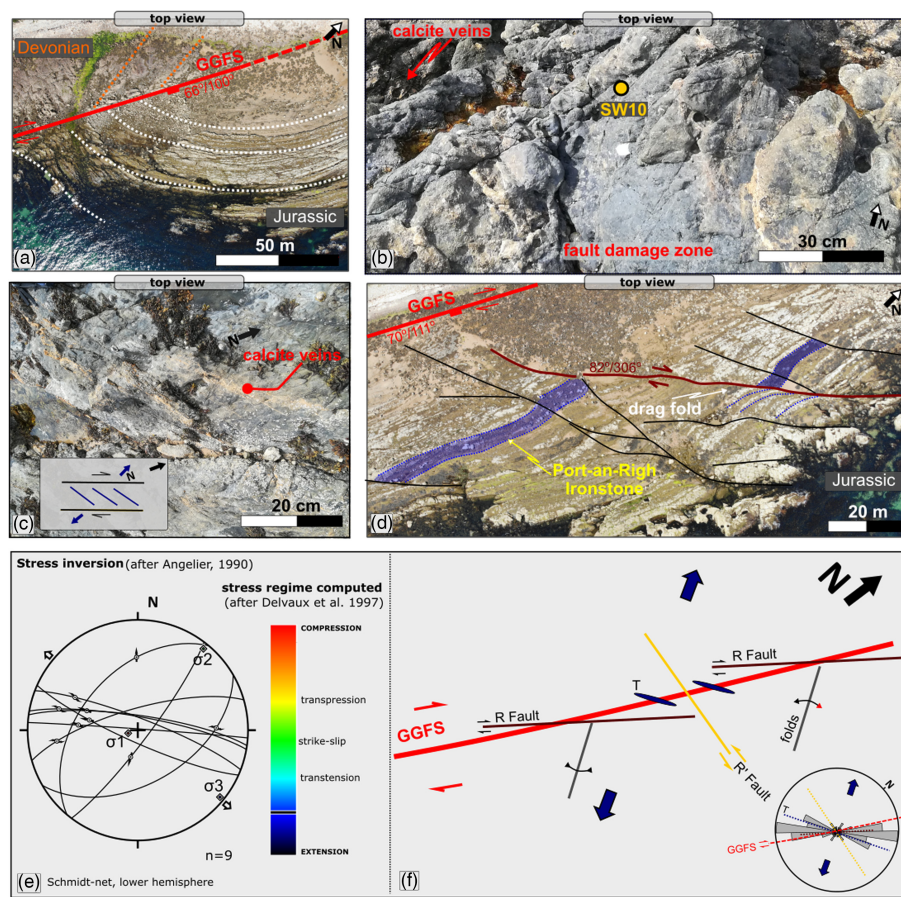


Fig. 8. (a) Drone photograph of the southern section of the Great Glen Fault (GGF) splay at Port an Righ (NH 85307 73253; see location in Fig. 7b) juxtaposing the Devonian rocks to the NW against Upper Jurassic strata to the SE (structural measurements provided as dip/dip direction). (b) Field photograph of the locally preserved damage zone associated with the GGF splay [NH 85473 73592]. Location of sample SW10 is also indicated. (c) Field photograph and inset sketch of the en echelon calcite-mineralized tensile veins associated with the dextral slip of the GGF splay. (d) Drone photograph showing a dextral high-angle fault displacing the Port an Righ Ironstone [NH 85496 73519], most likely representing a synthetic Riedel shear to the GGF splay (structural measurements are provided as dip/dip direction). (e) Stress inversion plot (after Angelier 1990) of fault lineation data. (f) Interpreted array of structures identified at Shandwick in map view and inset rose diagram of azimuth distributions. The fault array geometry and stress inversion analysis are consistent with dextral transension along the GGF splay. Structures are colour-coded in both the sketch and rose diagram as follows: dashed red line, main (GGF splay) fault; dark red line, synthetic Riedel shear (R); yellow, antithetic Riedel shear (R'); blue lines, tensile (T) fractures. GGFS, GGF splay.

dated in this work, lack such deformation features even where they occur in high strain zones (Fig. 9b).

Geochronology results

The ^{238}U and ^{206}Pb concentrations in the five fracture fills presented here contained sufficient amounts of ^{238}U (and low enough concentrations of common Pb, thus yielding $^{238}\text{U}/^{206}\text{Pb}$ ratios >1) to yield accurate and precise dates. The samples spatially associated with the Helmsdale Fault yielded both Late Jurassic and Early

Cretaceous dates (Fig. 10a–d). He01 yielded a $^{238}\text{U}/^{206}\text{Pb}$ age of 159.2 ± 11.5 Ma (2σ , MSWD = 2), whereas HD1, HELK01 and He03 gave $^{238}\text{U}/^{206}\text{Pb}$ ages of 126.3 ± 6.8 Ma (2σ , MSWD = 3.4), 119.3 ± 8.5 Ma (2σ , MSWD = 2) and 115.7 ± 19.4 Ma (2σ , MSWD = 1.8), respectively. At Shandwick, SW10 gave an Early Cretaceous date (Fig. 10e) with a $^{238}\text{U}/^{206}\text{Pb}$ age of 128.2 ± 42.4 Ma (2σ , MSWD = 1.9). The large uncertainty within the calculated age of this sample arises from the low $^{238}\text{U}/^{206}\text{Pb}$ ratios measured, resulting in a large uncertainty on the lower intercept that would be better constrained in a sample with higher $^{238}\text{U}/^{206}\text{Pb}$ ratios.

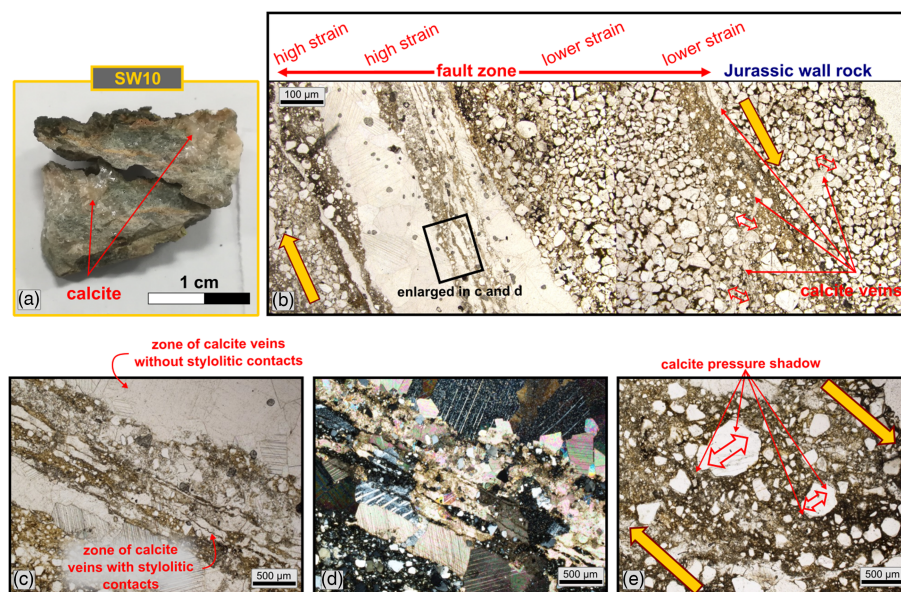


Fig. 9. (a) SW10 hand specimen collected from the GGF splay fault zone. (b–e) Representative thin section microphotographs. (b) Calcite veins that both predate and post-date faulting and are kinematically consistent with dextral shear (tensile jogs). (c, d) Earlier veins are cataclastically deformed and show stylolitic contacts, whereas the later veins are without stylolitic contacts developed in high strain areas. (e) Clasts in high strain regions showing obliquely oriented calcite pressure shadows.

Discussion

The structures seen in the Upper Jurassic rocks at Helmsdale are kinematically consistent with oblique-sinistral slip along the Helmsdale Fault, as proposed previously, but this has usually been attributed to Cenozoic reactivation during basin inversion and exhumation (Fig. 11; Le Breton *et al.* 2013). Our new U–Pb analyses of calcite mineral fills spatially associated with Helmsdale Fault yield two distinct ages: Late Jurassic (*c.* 159 Ma, Oxfordian) and Early Cretaceous (*c.* 126–115 Ma, Barremian–Aptian). Because the calcite veins cut the folds at Helmsdale, it has previously been assumed that they are younger features. However, the hinge-normal orientation of the veins is consistent with near-fold hinge-parallel finite extension during transtensional deformation (e.g. Venkat-Ramani and Tikoff 2002; Fossen *et al.* 2013). Hence an alternative explanation is that the sinistrally transtensional Helmsdale Fault, folds and veins are all related kinematically. The calcite fills therefore probably relate to two temporally distinct phases of sinistral movement along the basin-bounding fault, both of which are older than the Cenozoic. The two movement phases are consistent with the observed cross-cutting and contact relationships seen in the field and thin sections because the NE–SW-trending veins are clearly composite in nature (e.g. Fig. 5d, h).

The younger set of calcite fills at Helmsdale are the same Early Cretaceous age (within error) as the veins associated with the dextral GGF splay at Shandwick. Strike-slip faults and folds formed here during dextral movements along the main NNE–SSW structure. The dated veins are everywhere closely associated with these structures. Although the dated calcite fill here locally cross-cuts deformation structures related to dextral faults (Fig. 9b, c), it seems highly likely that the veining is related to this deformation. More importantly, the dated vein-fill here demonstrates that the strike-slip reactivation cannot be Cenozoic as has been proposed previously (e.g. Underhill and Brodie 1993; Le Breton *et al.* 2013; Fig. 11).

The Helmsdale Fault also preserves evidence for an early Late Jurassic (*c.* 159 Ma) phase of sinistral shear. This older date is within error of the postulated stratigraphic age of the Boulder Beds at Helmsdale (Kimmeridgian–Tithonian; e.g. Barron 1989), highlighting the need for a possible reappraisal of the precise stratigraphic age of the rocks. Alternatively, it may simply be that the veining occurred very soon after deposition and that the ages of sedimentation and veining simply cannot be separated based on the current resolution of the U–Pb dating method used here.

More generally, the Late Jurassic–Early Cretaceous U–Pb ages from Helmsdale and Shandwick broadly overlap with the timing of major tectonic events and rifting in the IMFB (Fig. 11), even though, strictly speaking, the younger set of Early Cretaceous ages (*c.* 128–115 Ma) corresponds to a period of subsidence according to some studies (e.g. Underhill 1991; Thomson and Underhill 1993; Davies *et al.* 2001). However, Andrews *et al.* (1990), Roberts *et al.* (1990) and Argent *et al.* (2002) suggested that some faults were longer lived, with movements as young as the Late Cretaceous. It is therefore plausible that this dated episode is the onshore expression of a late rifting pulse. The age range lies close to the 134.50 ± 19.4 Ma date obtained by Tamas *et al.* (2023) from dilational jog vein-fills associated with an ENE–WSW-trending fault located in the footwall of the Helmsdale Fault at Sarlet (Figs 1a, 11). The age range also lies close to the 130.99 ± 4.60 Ma U–Pb calcite age related to the dextral reactivation of a Devonian NNE–SSW-trending structure in New Aberdour (Turriff Sub-basin; Fig. 1a) on the southern margin of the IMFB (Tamas *et al.* 2022a; Fig. 11). It could be that these later Cretaceous movements are difficult to separate in offshore regions due to gaps in the coverage of seismic profiles and the limitations in the resolution of old 2D seismic profiles.

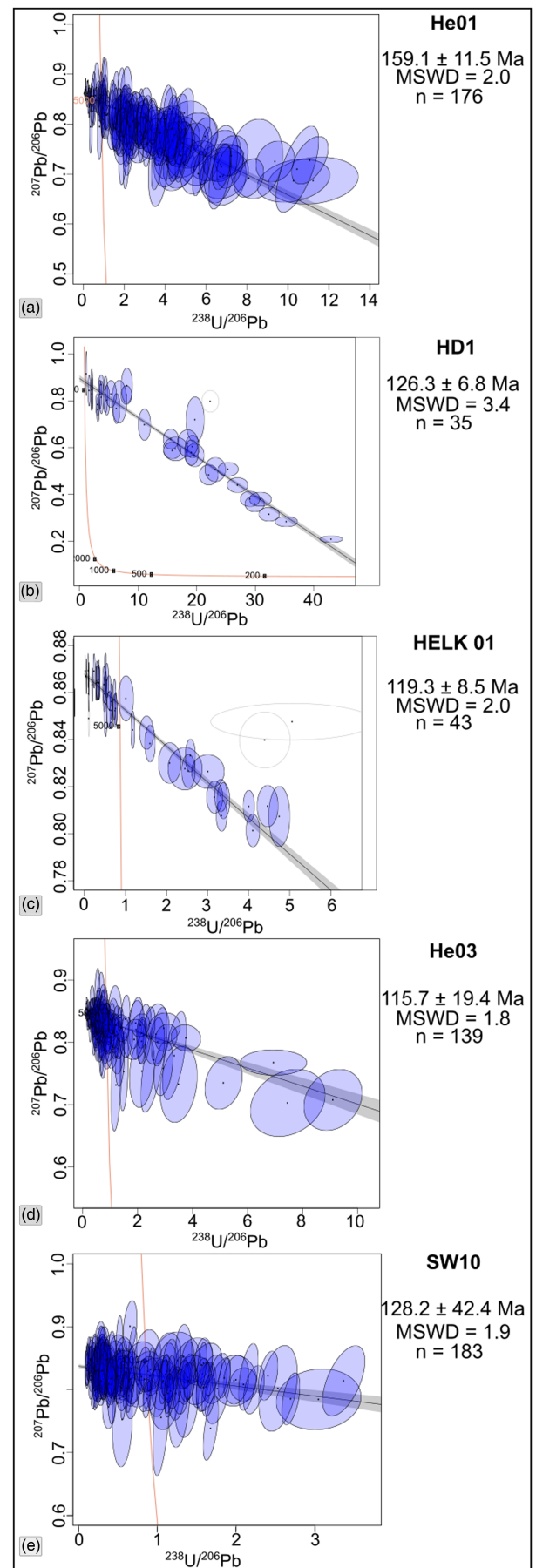


Fig. 10. Tera–Wasserburg plots of measured *in situ* calcite $^{207}\text{Pb}/^{206}\text{Pb}$ and $^{238}\text{U}/^{206}\text{Pb}$ ratios.

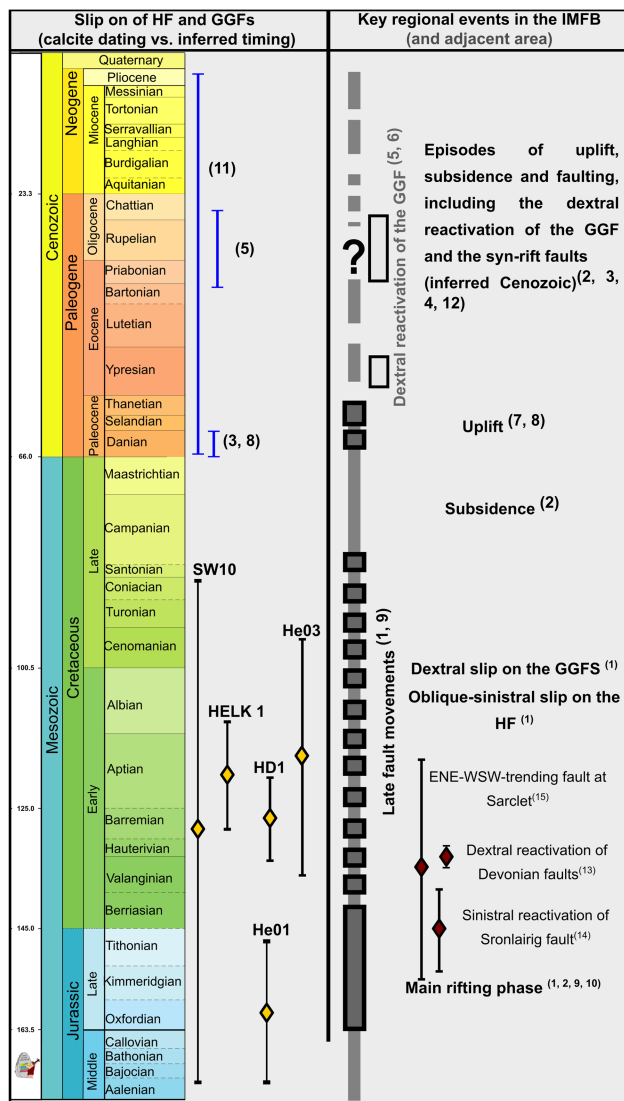


Fig. 11. Summary of dating results against local and key regional events after (1) present study, (2) Underhill (1991), (3) Thomson and Hillis (1995), (4) Zanella and Coward (2003), (5) Le Breton *et al.* (2013), (6) Holgate (1969), (7) Argent *et al.* (2002), (8) Hillis *et al.* (1994), (9) Andrews *et al.* (1990), (10) Davies *et al.* (2001), (11) Underhill and Brodie (1993), (12) Tamas *et al.* (2022b), (13) Tamas *et al.* (2022a), (14) Kemp *et al.* (2019), (15) Tamas *et al.* (2023). GGF, Great Glen Fault; GGFS, Great Glen Fault splay at Shandwick; HF, Helmsdale Fault; IMFB, Inner Moray Firth Basin.

Further afield, Kemp *et al.* (2019) used K–Ar dating on fault gouges associated with the Sronlairig Fault, an ENE–WSW-trending sinistral fault related to the GGF near Loch Ness (Fig. 1a). This revealed a Late Carboniferous–Early Permian age (296 ± 7 Ma) and a Late Jurassic–Early Cretaceous age of 145 ± 7 Ma. These researchers proposed that the later date corresponds to a relatively late movement along this fault related to the main phase of opening of the IMFB, a suggestion that seems to be broadly in line with the findings reported here (Fig. 11).

It remains to be seen whether there is any direct onshore evidence for Cenozoic movements along either the Helmsdale Fault or the GGF splay on the northern margin of the IMFB. There are known to be significant Cenozoic right-lateral movements along the main part of the GGF, which lies offshore and to the south. Right-lateral displacements are estimated to be *c.* 30 km based on the offset of Cenozoic dykes in Scotland (Holgate 1969) and are more generally associated with regional tilting and uplift of the IMFB. Tamas *et al.* (2022b) recognized significant Cenozoic reactivation along faults in the southern marginal parts of the IMFB (e.g. the Lossiemouth and Clashach faults). Significantly, movements along those faults exposed onshore are associated with widespread hematite mineralization and not calcite precipitation.

In the case of the GGF splay at Shandwick, it may be that this fault strand was abandoned during the Cenozoic dextral reactivation of the GGF (Fig. 12). This pattern is commonly associated with the development and growth of basement-controlled strike-slip fault zones (e.g. Naylor *et al.* 1986; Richard *et al.* 1995; de Jossineau and Aydin 2007). Analogue models typically suggest that basement-controlled strike-slip faulting creates sequential en echelon Riedel shears in the overlying cover rocks. With increased displacement, some segments join to form a thorough-going fault zone, whereas others are abandoned, which could be the case for the GGF splay at Shandwick during Cenozoic reactivation (Fig. 12).

Conclusions and implications

U–Pb dating of syn- to post-kinematic calcite mineralization associated with the northern margin of the IMFB shows that significant transensional reactivation occurred along the basin-bounding Helmsdale Fault (sinistral) and a splay of the GGF (dextral) during the Early Cretaceous (128–115 Ma). The Helmsdale Fault also preserves evidence for an earlier Late Jurassic (*c.* 159 Ma) phase of sinistral shear. The fault movement ages obtained here are not compatible with most previous studies (e.g. Thomson and Underhill 1993; Le Breton *et al.* 2013). We do not rule out the possibility that Cenozoic fault movements have occurred in the IMFB, but our new data show that a significant

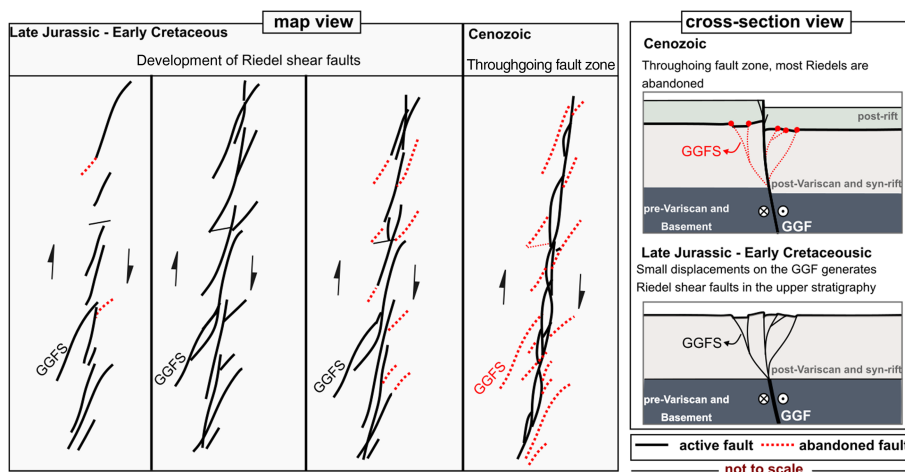


Fig. 12. Conceptual diagram explaining the sequential evolution of the Great Glen Fault and splay during syn- and post-rift reactivation (adapted after Naylor *et al.* 1986). (a) Map view; (b) cross-section. GGF, Great Glen Fault; GGFS, Great Glen Fault splay.

proportion of the deformation along these faults where they are seen onshore is much older than the Cenozoic. It appears that the Mesozoic opening of the IMFB is more than a simple, single phase of NW–SE orthogonal rifting. Our findings demonstrate that the mesoscale reactivation of inherited structures is widespread, leading to repeated local transtensional deformation episodes comparable with those recognized by Tamas *et al.* (2022a, b) along the southern margin of the IMFB. Such oblique-slip faults are rarely recognized unequivocally in the subsurface because they require good 3D imaging and usually need to refer to analogue experiments to validate interpretation. We therefore hope that this study will inspire subsurface interpreters to reconsider the possible importance of oblique-slip deformation patterns in other superimposed rift basins.

Scientific editing by Yildirim Dilek

Acknowledgements Reviewer Catherine Mottram and Editor Yildirim Dilek are thanked for their constructive and helpful comments.

Author contributions AT: conceptualization (equal), data curation (lead), formal analysis (lead), investigation (lead), methodology (equal), software (lead), visualization (lead), writing – original draft (equal); REH: conceptualization (equal), funding acquisition (equal), methodology (equal), supervision (lead), validation (lead), writing – original draft (equal), writing – review and editing (equal); DMT: data curation (supporting), investigation (supporting), methodology (equal), software (equal), visualization (supporting), writing – review and editing (supporting); EDD: investigation (supporting), methodology (equal), software (supporting), supervision (supporting), writing – review and editing (equal); KH: methodology (supporting), software (supporting), visualization (supporting), writing – review and editing (supporting); AB: methodology (supporting), software (supporting), visualization (supporting), writing – review and editing (supporting); NMWR: formal analysis (supporting), methodology (equal), software (equal), visualization (equal), writing – review and editing (supporting); JL: methodology (supporting), software (supporting), visualization (supporting), writing – review and editing (supporting); JRJ: conceptualization (supporting), funding acquisition (equal), supervision (equal), validation (supporting), writing – review and editing (supporting); DM: funding acquisition (equal), supervision (supporting), validation (supporting), writing – review and editing (supporting); KJWM: supervision (supporting), validation (supporting), writing – review and editing (supporting); DS: supervision (supporting), validation (supporting), writing – review and editing (supporting).

Funding This paper is based on the PhD work of AT undertaken as part of the Natural Environment Research Council Centre for Doctoral Training in Oil and Gas (NEM00578X/1) and was funded by Durham University and the British Geological Survey, whose support is gratefully acknowledged.

Competing interests The authors declare that they have no known competing financial interests or personal relationships that could have appeared to influence the work reported in this paper.

Data availability All data generated or analysed during this study are included in this published article (and its supplementary information files).

References

- Andrews, I.J., Long, D., Richards, P.C., Thomson, A.R., Brown, S., Chesher, J.A. and McCormac, M. 1990. *The Geology of the Moray Firth*. United Kingdom Offshore Regional Report. British Geological Survey, London.
- Angelier, J. 1990. Inversion of field data in fault tectonics to obtain the regional stress III: a new rapid direct inversion method by analytical means. *Geophysical Journal International*, **103**, 363–376, <https://doi.org/10.1111/j.1365-246X.1990.tb01777.x>
- Argent, J., Stewart, S.A., Green, P. and Underhill, J.R. 2002. Heterogeneous exhumation in the Inner Moray Firth, UK North Sea: constraints from new apatite fission track analysis and seismic data. *Journal of the Geological Society, London*, **159**, 715–729, <https://doi.org/10.1144/0016-764901-141>
- Bailey, E.B. and Weir, J. 1932. Submarine faulting in Kimmeridgian times: East Sutherland. *Transactions of the Royal Society of Edinburgh*, **57**, 429–467, <https://doi.org/10.1017/S0080456800016768>
- Barron, H.F. 1989. Dinoflagellate cyst biostratigraphy and paleoenvironments of the Upper Jurassic (Kimmeridgian to basal Portlandian) of the Helmsdale region, east Sutherland, Scotland. In: Batten, D.J. and Keen, M.C. (eds) *Northwest European Micropalaeontology and Palynology*. Ellis Horwood for the British Micropalaeontological Society, Chichester, 193–213.
- BGS 1998. *Geological Map, Helmsdale, Scotland Sheet 103E, 1:50,000*. British Geological Survey, Keyworth.
- Cardozo, N. and Allmendinger, R.W. 2013. Spherical projections with OSXstereonet. *Computers & Geosciences*, **51**, 193–205, <https://doi.org/10.1016/j.cageo.2012.07.021>
- Coward, M.P., Enfield, M.A. and Fischer, M.W. 1989. Devonian basins of northern Scotland: extension and inversion related to Late Caledonian–Variscan tectonics. *Geological Society, London, Special Publications*, **44**, 275–308, <https://doi.org/10.1144/GSL.SP.1989.044.01.16>
- Davies, R.J., Turner, J.D. and Underhill, J.R. 2001. Sequential dip-slip fault movement during rifting: a new model for the evolution of the Jurassic trilete North Sea rift system. *Petroleum Geoscience*, **7**, 371–388, <https://doi.org/10.1144/petgeo.7.4.371>
- de Jossineau, G. and Aydin, A. 2007. The evolution of the damage zone with fault growth in sandstone and its multiscale characteristics. *Journal of Geophysical Research*, **112**, B12401, <https://doi.org/10.1029/2006JB004711>
- De Paola, N., Holdsworth, R.E., McCaffrey, K.J.W. and Barchi, M.R. 2005. Partitioned transtension: an alternative to basin inversion models. *Journal of Structural Geology*, **27**, 607–625, <https://doi.org/10.1016/j.jsg.2005.01.006>
- Dewey, J.F. and Strachan, R.A. 2003. Changing Silurian–Devonian relative plate motion in the Caledonides: sinistral transpression to sinistral transtension. *Journal of the Geological Society, London*, **160**, 219–229, <https://doi.org/10.1144/0016-764902-085>
- Dichiarante, A.M., Holdsworth, R.E. *et al.* 2016. New structural and Re–Os geochronological evidence constraining the age of faulting and associated mineralization in the Devonian Orcadian Basin, Scotland. *Journal of the Geological Society, London*, **173**, 457–473, <https://doi.org/10.1144/jgs2015-118>
- Dichiarante, A.M., McCaffrey, K.J.W., Holdsworth, R.E., Björnå, T.I. and Dempsey, E.D. 2020. Fracture attribute scaling and connectivity in the Devonian Orcadian Basin with implications for geologically equivalent subsurface fractured reservoirs. *Solid Earth*, **11**, 2221–2244, <https://doi.org/10.5194/se-11-2221-2020>
- Duxbury, S. and Vieira, M. 2018. A stratigraphic review of the Late Callovian to Oxfordian Interval, Fisher Bank Basin Area (UK Sector, Central North Sea). *Journal of Petroleum Geology*, **41**, 47–65, <https://doi.org/10.1111/jpg.12692>
- Fossen, H., Teyssier, C. and Whitney, D.L. 2013. Transtensional folding. *Journal of Structural Geology*, **56**, 89–102, <https://doi.org/10.1016/j.jsg.2013.09.004>
- Hillis, R.R., Thomson, K. and Underhill, J.R. 1994. Quantification of Tertiary erosion in the Inner Moray Firth using sonic velocity data from the Chalk and the Kimmeridge Clay. *Marine and Petroleum Geology*, **11**, 283–293, [https://doi.org/10.1016/0264-8172\(94\)90050-7](https://doi.org/10.1016/0264-8172(94)90050-7)
- Holdsworth, R.E., Trice, R. *et al.* 2020. The nature and age of basement host rocks and fissure fills in the Lancaster field fractured reservoir, west of Shetland. *Journal of the Geological Society, London*, **177**, 1057–1073, <https://doi.org/10.1144/jgs2019-142>
- Holgate, N. 1969. Palaeozoic and Tertiary transcurrent movements on the Great Glen fault. *Scottish Journal of Geology*, **5**, 97–139, <https://doi.org/10.1144/sjg05020097>
- Kemp, S., Gillespie, M., Leslie, G., Zwingmann, H. and Campbell, S. 2019. Clay mineral dating of displacement on the Sronlairig Fault: implications for Mesozoic and Cenozoic tectonic evolution in northern Scotland. *Clay Minerals*, **54**, 181–196, <https://doi.org/10.1180/clm.2019.25>
- Le Breton, E., Cobbold, P.R. and Zanella, A. 2013. Cenozoic reactivation of the Great Glen Fault, Scotland: additional evidence and possible causes. *Journal of the Geological Society, London*, **170**, 403–415, <https://doi.org/10.1144/jgs2012-067>
- MacDonald, A.C. 1985. *Kimmeridgian and Volgian Fault-Margin Sedimentation in the Northern North Sea Area*. PhD thesis, University of Strathclyde.
- MacDonald, A.C. and Trewin, N.H. 2009. The Upper Jurassic of the Helmsdale area. In: Trewin, N. and Hurst, A. (eds) *Excursion Guide to the Geology of East Sutherland and Caithness*. 2nd edn. Aberdeen Geological Society and Dunedin Press, Edinburgh, 74–107.
- McArthur, A.D., Hartley, A.J. and Jolley, D.W. 2013. Stratigraphic development of an Upper Jurassic deep marine syn-rift succession, Inner Moray Firth Basin, Scotland. *Basin Research*, **25**, 285–309, <https://doi.org/10.1111/j.1365-2117.2012.00557.x>
- McQuillan, R., Donato, J.A. and Tulstrup, J. 1982. Development of basins in the Inner Moray Firth and the North Sea by crustal extension and dextral displacement of the Great Glen Fault. *Earth and Planetary Science Letters*, **60**, 127–139, [https://doi.org/10.1016/0012-821X\(82\)90028-0](https://doi.org/10.1016/0012-821X(82)90028-0)
- Mendum, J.R. and Noble, S.R. 2010. Mid-Devonian sinistral transpressional movements on the Great Glen Fault: the rise of the Rosemarkie Inlier and the Acadian Event in Scotland. *Geological Society, London, Special Publications*, **335**, 161–187, <https://doi.org/10.1144/SP335.8>
- Naylor, M.A., Mandl, G. and Supesteijn, C.H.K. 1986. Fault geometries in basement-induced wrench faulting under different initial stress states. *Journal of Structural Geology*, **8**, 737–752, [https://doi.org/10.1016/0191-8141\(86\)90022-2](https://doi.org/10.1016/0191-8141(86)90022-2)
- Pickering, K.T. 1984. The Upper Jurassic ‘Boulder Beds’ and related deposits: a fault-controlled submarine slope, NE Scotland. *Journal of the Geological Society, London*, **141**, 357–374, <https://doi.org/10.1144/gsjgs.141.2.0357>

- Richard, P.D., Naylor, M.A. and Koopman, A. 1995. Experimental models of strike-slip tectonics. *Petroleum Geoscience*, **1**, 71–80, <https://doi.org/10.1144/petgeo.1.1.71>
- Riding, J.B. 2005. Middle and Upper Jurassic (Callovian to Kimmeridgian) palynology of the onshore Moray Firth Basin, northeast Scotland. *Palynology*, **29**, 87–142, <https://doi.org/10.2113/29.1.87>
- Roberts, A.M., Badley, M.E., Price, J.D. and Huck, I.W. 1990. The structural history of a transtensional basin: Inner Moray Firth, NE Scotland. *Journal of the Geological Society, London*, **147**, 87–103, <https://doi.org/10.1144/gsjgs.147.1.0087>
- Roberts, N.M.W. and Holdsworth, R.E. 2022. Timescales of faulting through calcite geochronology: a review. *Journal of Structural Geology*, **158**, <https://doi.org/10.1016/j.jsg.2022.104578>
- Roberts, N.M.W., Troy Rasbury, E., Parrish, R.R., Smith, C.J., Horstwood, M.S.A. and Condon, D.J. 2017. A calcite reference material for LA-ICP-MS U–Pb geochronology. *Geochemistry, Geophysics, Geosystems*, **18**, 2807–2814, <https://doi.org/10.1002/2016GC006784>
- Sasvári, Á. and Baharev, A. 2014. SG2PS (structural geology to postscript converter) – a graphical solution for brittle structural data evaluation and paleostress calculation. *Computers & Geosciences*, **66**, 81–93, <https://doi.org/10.1016/j.cageo.2013.12.010>
- Salomon, E., Rotevatn, A. *et al.* 2020. Fault-controlled fluid circulation and diagenesis along basin-bounding fault systems in rifts – insights from the East Greenland rift system. *Solid Earth*, **11**, 1987–2013, <https://doi.org/10.5194/se-11-1987-2020>
- Stephen, K.J., Underhill, J.R., Partington, M. and Hedley, R.J. 1993. The genetic sequence stratigraphy of the Hettangian to Oxfordian sedimentary succession, Inner Moray Firth. *Geological Society, London, Petroleum Geology Conference Series*, **4**, 485–505, <https://doi.org/10.1144/0040485>
- Stewart, M., Strachan, R.A., Martin, M.W. and Holdsworth, R.E. 2001. Constraints on early sinistral displacements along the Great Glen Fault Zone, Scotland: structural setting, U–Pb geochronology and emplacement of the syn-tectonic Clunes tonalite. *Journal of the Geological Society, London*, **158**, 821–830, <https://doi.org/10.1144/jgs.158.5.821>
- Tamas, D.M., Tamas, A., Barabasch, J., Rowan, M.G., Schleder, Z., Krézsek, C. and Urai, J.L. 2021. Low-angle shear within the exposed Mánzâlești diapir, Romania: salt decapitation in the Eastern Carpathians fold-and-thrust belt. *Tectonics*, **40**, e2021TC006850, <https://doi.org/10.1029/2021TC006850>
- Tamas, A., Holdsworth, R.E. *et al.* 2022a. New onshore insights into the role of structural inheritance during Mesozoic opening of the Inner Moray Firth Basin, Scotland. *Journal of the Geological Society, London*, **179**, jgs2021-066, <https://doi.org/10.1144/jgs2021-066>
- Tamas, A., Holdsworth, R.E. *et al.* 2022b. Correlating deformation events onshore and offshore in superimposed rift basins: the Lossiemouth Fault Zone, Inner Moray Firth Basin, Scotland. *Basin Research*, **34**, 1314–1340, <https://doi.org/10.1111/bre.12661>
- Tamas, A., Holdsworth, R. *et al.* 2023. Using UAV-based photogrammetry coupled with in situ fieldwork and U–Pb geochronology to decipher multi-phase deformation processes: a case study from Sarclet, Inner Moray Firth Basin, UK. *Remote Sensing*, **15**, 695, <https://doi.org/10.3390/rs15030695>
- Thomson, K. and Hillis, R.R. 1995. Tertiary structuration and erosion of the Inner Moray Firth. *Geological Society, London, Special Publications*, **90**, 249–269, <https://doi.org/10.1144/GSL.SP.1995.090.01.16>
- Thomson, K. and Underhill, J.R. 1993. Controls on the development and evolution of structural styles in the Inner Moray Firth Basin. *Geological Society, London, Petroleum Geology Conference Series*, **4**, 1167–1178, <https://doi.org/10.1144/0041167>
- Trewin, N. 2009. The Triassic and Lower Jurassic of Golspie. In: Trewin, N. and Hurst, A. (eds) *Excursion Guide to the Geology of East Sutherland and Caithness*. 2nd edn. Aberdeen Geological Society and Dunedin Press, Edinburgh, 41–47.
- Trewin, N. and Hurst, A. (eds) 2009. *Excursion Guide to the Geology of East Sutherland and Caithness*. 2nd edn. Aberdeen Geological Society and Dunedin Press.
- Underhill, J.R. 1991. Implications of Mesozoic–Recent basin development in the western Inner Moray Firth, UK. *Marine and Petroleum Geology*, **8**, 359–369, [https://doi.org/10.1016/0264-8172\(91\)90089-J](https://doi.org/10.1016/0264-8172(91)90089-J)
- Underhill, J.R. and Brodie, J.A. 1993. Structural geology of Easter Ross, Scotland: implications for movement on the Great Glen fault zone. *Journal of the Geological Society, London*, **150**, 515–527, <https://doi.org/10.1144/gsjgs.150.3.0515>
- Venkat-Ramani, M. and Tikoff, B. 2002. Physical models of transtensional folding. *Geology*, **30**, 523–526, [https://doi.org/10.1130/0091-7613\(2002\)030<0523:PMOTF>2.0.CO;2](https://doi.org/10.1130/0091-7613(2002)030<0523:PMOTF>2.0.CO;2)
- Vermeesch, P. 2018. IsoplotR: a free and open toolbox for geochronology. *Geoscience Frontiers*, **9**, 1479–1493, <https://doi.org/10.1016/j.gsf.2018.04.001>
- Watts, L.M., Holdsworth, R.E., Sleight, J.A., Strachan, R.A. and Smith, S.A.F. 2007. The movement history and fault rock evolution of a reactivated crustal-scale strike-slip fault: the Walls Boundary Fault Zone, Shetland. *Journal of the Geological Society, London*, **164**, 1037–1058, <https://doi.org/10.1144/0016-76492006-156>
- Worthington, R.P. and Walsh, J.J. 2016. Timing, growth and structure of a reactivated basin-bounding fault. *Geological Society, London, Special Publications*, **439**, 511–531, <https://doi.org/10.1144/SP439.14>
- Zanella, E. and Coward, M.P. 2003. Structural framework. In: Evans, D., Graham, C., Armour, A. and Bathurst, P. (eds) *The Millennium Atlas: Petroleum Geology of the Central and Northern North Sea*. Geological Society Publishing House, Bath, 45–59.